A Relative Sea Surface Temperature Index for Classifying ENSO Events in a Changing Climate

MICHELLE L. L'HEUREUX,[a] MICHAEL K. TIPPETT,[b] MATTHEW C. WHEELER,[c] HANH NGUYEN,[c] SUGATA NARSEY,[c] NATHANIEL JOHNSON,[d] ZENG-ZHEN HU,[a] ANDREW B. WATKINS,[c] CHRIS LUCAS,[c] CATHERINE GANTER,[c] EMILY BECKER,[e] WANQIU WANG,[a] AND TOM DI LIBERTO[f]

[a] *NOAA/NWS/NCEP/Climate Prediction Center, College Park, Maryland*
[b] *Department of Applied Physics and Applied Mathematics, Columbia University, New York, New York*
[c] *Bureau of Meteorology, Melbourne, Victoria, Australia*
[d] *NOAA/OAR/Geophysical Fluid Dynamics Laboratory, Princeton, New Jersey*
[e] *University of Miami/Cooperative Institute for Marine and Atmospheric Studies, Miami, Florida*
[f] *NOAA Office of Communications, Washington, D. C.*

(Manuscript received 5 July 2023, in final form 3 November 2023, accepted 1 December 2023)

ABSTRACT: El Niño–Southern Oscillation (ENSO) is often characterized through the use of sea surface temperature (SST) departures from their climatological values, as in the Niño-3.4 index. However, this approach is problematic in a changing climate when the climatology itself is varying. To address this issue, van Oldenborgh et al. proposed a relative Niño-3.4 SST index, which subtracts the tropical mean SST anomaly from the Niño-3.4 index and multiplies by a scaling factor. We extend their work by providing a simplified calculation procedure for the scaling factor, and confirm that the relative index demonstrates reduced sensitivity to climate change and multidecadal variability. In particular, we show in three observational SST datasets that the relative index provides a more consistent classification of historical El Niño and La Niña oceanic conditions that is more robust across climatological periods compared to the nonrelative index. Forecast skill of the relative Niño-3.4 index in the North American Multimodel Ensemble (NMME) and ACCESS-S2 is slightly reduced for targets during the first half of the year because subtracting the tropical mean removes a source of additional skill. For targets in the second half of the year, the relative and nonrelative indices are equally skillful. Observed ENSO teleconnections in 200-hPa geopotential height and precipitation during key seasons are sharper and explain more variability over Australia and the contiguous United States when computed with the relative index. Overall, the relative Niño-3.4 index provides a more robust option for real-time monitoring and forecasting ENSO in a changing climate.

SIGNIFICANCE STATEMENT: The goal of this study is to further explore a relative sea surface temperature index for monitoring and prediction of El Niño–Southern Oscillation. Sea surface temperature indices are typically computed as a difference from a 30-yr climatological average, and El Niño and La Niña events occur when values exceed a certain threshold. This method is suitable when the climate is stationary. However, because of climate change and other lower-frequency variations, historical El Niño and La Niña events are reclassified depending on which climatological period is selected. A relative index is investigated to ameliorate this problem.

KEYWORDS: ENSO; Climate variability; Trends; Tropical variability

1. Introduction

El Niño–Southern Oscillation (ENSO) derives its name from the oceanic (El Niño) and atmospheric (Southern Oscillation) coupling that takes place periodically over the tropical Pacific Ocean. Because ENSO is a sprawling, diverse, and multifaceted coupled ocean–atmosphere phenomenon (Bjerknes 1969), there are many different indices that measure it (Li et al. 2023). While all metrics provide some insight into ENSO, arguably the most widely used index is the Niño-3.4 index, which is based on the departure of sea surface temperature (SST) averaged over the Niño-3.4 region (5°S–5°N, 170°–120°W) from its climatological value (Barnston et al. 1997). Even though ENSO is a coupled atmosphere–ocean phenomenon, oceanic indices such as the Niño-3.4 index are less affected by shorter-term weather fluctuations compared to atmospheric indices, making it more smoothly varying and more amenable for real-time monitoring. The Niño-3.4 index therefore plays a key role in early alert systems for El Niño and La Niña from operational climate centers, such as the National Oceanic and Atmospheric Administration (NOAA) Climate Prediction Center (CPC) in the United States and the Bureau of Meteorology (BOM) in Australia (Nguyen et al. 2022). For these alerts, Niño-3.4 thresholds of ±0.5°C (NOAA) and 0.8°C (BOM), along with other measures of the tropical atmospheric circulation (Southern Oscillation index, outgoing longwave radiation anomalies, wind anomalies, etc.; Gamble et al. 2017; L'Heureux et al. 2017) are used to define the ENSO status. Such thresholds are important for users who

Supplemental information related to this paper is available at the Journals Online website: https://doi.org/10.1175/JCLI-D-23-0406.s1.

Corresponding author: Michelle L. L'Heureux, michelle.lheureux@noaa.gov

DOI: 10.1175/JCLI-D-23-0406.1

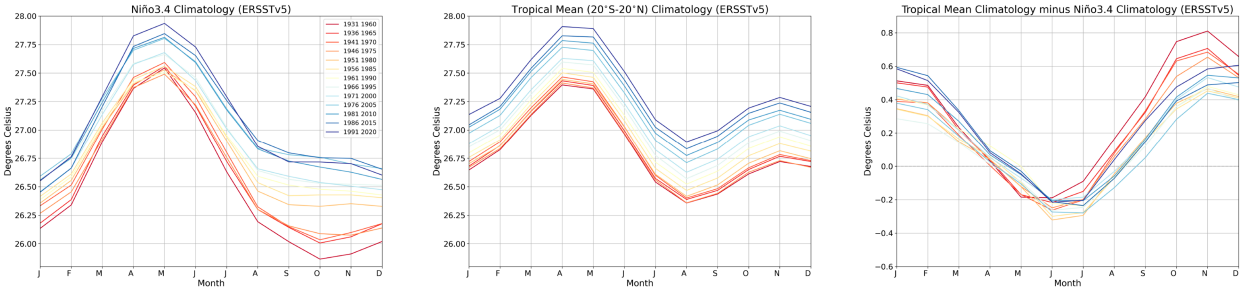

FIG. 1. Overlapping 30-yr climatologies over 1931–2020 for (left) monthly mean values of Niño-3.4 and (center) the tropical mean (20°S–20°N), and (right) the difference between the tropical mean and Niño-3.4. Units are in °C (*y* axis) and shown by calendar month (*x* axis). Data are from ERSSTv5.

make decisions on whether to mobilize resources to prepare for El Niño or La Niña events and therefore desire an objective, governmentally endorsed ENSO definition.

Defining ENSO events based on anomalies (departures from the mean) necessitates defining a climatology or a baseline average, from which SST anomalies are calculated. Conventionally, the BOM and CPC have followed practices from the World Meteorological Organization (WMO) recommendation to compute climate anomalies with respect to a single 30-yr monthly mean climatology (WMO 2017). The assumption is that a 30-yr period is long enough to average out most interannual-to-decadal climate variability, including that of ENSO. However, in a warming climate there are pronounced shifts in the climatology of the Niño-3.4 region from one 30-yr period to another (Fig. 1, left panel). Consequently, whether the magnitudes of Niño-3.4 index exceed thresholds or not is increasingly dependent on the climatology used. On the other hand, ENSO is a physical phenomenon and an inherent mode of seasonal-to-interannual global climate variability, and therefore ENSO classification should ideally be independent of the choice of climatology. For example, the lived experience of an El Niño or La Niña event during the 1950s should not be modified based on a warmer climatology that occurs 70 years later (e.g., 1991–2020).

Recognizing that trends in the Niño-3.4 index influence the categorization of El Niño and La Niña events, van Oldenborgh et al. (2021) defined a relative SST index for ENSO monitoring. This index is based on the difference of the Niño-3.4 index (SST anomalies averaged in the region 5°S–5°N, 120°–170°W) and a tropical mean index (SST anomalies over the entire tropics, from 20°S to 20°N). A scaling factor is applied to the difference to match the variance of the Niño-3.4 index. Van Oldenborgh et al. (2021) argued that this relative Niño-3.4 index has several advantages over the current NOAA method of computing the Oceanic Niño Index (ONI), which is the 3-month (seasonal) running mean of the Niño-3.4 index. Currently, the ONI is computed as a departure from a moving 30-yr climatology that updates every 5 years, which means that the most recent 15 years of ONI values are changed every five years when those updates occur (NOAA CPC 2023). Further, van Oldenborgh et al. (2021) demonstrated that the relative SST index more effectively removes trends in the recent, real-time record when a past 30-yr climatology is used. One consequence of this lagged climatology is that the humanitarian response to the La Niña of 2016/17 (declared by NOAA but not by BOM) may have been more limited because ONI values were with respect to the 1986–2015 climatology, which made them warmer than they would have been had a centered climatology been used. In this case, the weak La Niña event suggested by the real-time ONI values did not match the impacts that ultimately occurred (van Oldenborgh et al. 2021).

Beyond its use for ENSO applications, another reason adopting a relative SST index is warranted in a changing climate is that it is more directly associated with local atmospheric instability. Local instability in turn is more directly tied to rainfall and convective anomalies, which are key to the coupled ocean–atmosphere ENSO phenomenon. Mainly, the relative Niño-3.4 index more closely reflects the changes in the tropical Pacific SST gradients that drive Walker circulation changes and hence atmosphere–ocean coupling, and, unlike the conventional Niño-3.4 index, its formulation is more directly associated with local atmospheric instability.

Why is a relative index more directly tied to local instability? Due to the small Coriolis effect near the equator, there is little horizontal variation in temperature in the upper tropical troposphere (Sobel et al. 2002). Therefore, the surface conditions across the entire tropics set the temperature of the troposphere beyond the boundary layer. The tropical mean SST is, in essence, a proxy for tropospheric temperature, and the difference of tropospheric and local surface temperatures controls instability, which explains why the relative Niño-3.4 index is better tied to changes in tropical deep convection (Back and Bretherton 2009; Johnson and Xie 2010; Johnson and Kosaka 2016; Izumo et al. 2020). In fact, this reasoning is also provided to justify using relative SSTs to determine tropical cyclone potential intensity (Vecchi and Soden 2007; Ramsay and Sobel 2011). Because relative SST has a physical basis, it is preferred compared to subtracting out a curve or least squares trend fit line placed through the Niño-3.4 index. The latter strategy would be especially challenging to apply to real-time monitoring when it is not clear that the fit can be reliably extrapolated, although alternative methods involving trend removal have been proposed (Turkington et al. 2019).

While van Oldenborgh et al. (2021) provided compelling arguments for using a relative index for ENSO monitoring, a number of practical issues and questions remained. In the analysis

that follows, we propose a simpler method of computing the scaling factor in the relative Niño-3.4 index, which eases the computation of the relative index in model forecasts and simulations. We also extend the van Oldenborgh et al. (2021) index computation using the NOAA extended reconstruction SSTs version 5 (ERSSTv5) and compare it with two other well-known SST datasets: the Hadley Centre Global Sea Ice and SST (HadISST) and the Centennial in situ Observation-Based Estimates (COBE) SST. While van Oldenborgh et al. (2021) briefly examined the forecast skill of the relative index using the European Centre for Medium-Range Weather Forecasts (ECMWF) model, we perform a more extensive forecast verification using multiple models. Finally, we take a closer examination of ENSO teleconnections, in 200-hPa geopotential height and precipitation, to assess the ability of the relative index to identify an ENSO signal with less influence from climate change and multidecadal variability. Overall, we find that the relative SST index provides a more stable historical record of El Niño and La Niña events that is not as sensitive to changes in climatology or the choice of SST dataset.

2. Data and methods

In addition to the NOAA ERSSTv5 data (Huang et al. 2017) that van Oldenborgh et al. (2021) examined, the Met Office Hadley SST (Rayner et al. 2003) and Japan Meteorological Agency (JMA) COBE SST (Ishii et al. 2005) datasets are also examined and used to compute the Niño-3.4 and tropical mean indices, as discussed in the previous section. Focusing on ERSSTv5, Fig. 1 herein shows the monthly mean climatology of total SST in the two regions for multiple overlapping 30-yr periods (left and center panels) and the difference between them (right panel). Figure 1 in the online supplemental material repeats this figure for the HadSST and COBE SST datasets. Notably, across all three datasets, the seasonality of the Niño-3.4 region and the tropical mean region is not the same, which results in up to 0.8°C difference between the climatologies of the two different regions. Therefore, in order to avoid including a seasonal cycle in the relative Niño-3.4 index, the monthly mean climatology of tropical mean SST and Niño.3.4 SST must be subtracted prior to the computation of the relative Niño-3.4 index. We tested different ranges of latitudes (15°–30°) to define the tropical mean with similar differences found in the seasonality (not shown). We selected 20°S–20°N as in van Oldenborgh et al. (2021).

In addition to examining multiple observational SST datasets, seven climate models are evaluated for their skill in predicting indices of Niño-3.4, tropical mean, and relative Niño-3.4 for all calendar month targets and forecast lead times (out to 8–12-month lead times). Herein, 0-month forecast lead refers to the monthly average closest to the initial condition, which occurs during the first week of the month (for some models, some members are lagged with conditions extending back to the final week of the previous month). Six of these models come from the North American Multimodel Ensemble (NMME) prediction system, which is often relied upon in operational ENSO predictions by NOAA (Kirtman et al. 2014; Becker et al. 2022). Models are sourced from the National Aeronautics and Space Administration (NASA), Environment and Climate Change Canada (ECCC), and two groups from the National Oceanic and Atmospheric Administration (NOAA): the National Centers for Environmental Prediction (NCEP) and the Geophysical Fluid Dynamics Laboratory (GFDL). The University of Miami also provides a model (CCSM4) and leads the NMME research project. Additionally, the ACCESS-S2 global coupled model, as used operationally for multiweek to seasonal prediction at the BOM, is also evaluated (Wedd et al. 2022). The NMME models are evaluated over the period from 1991 to 2022 because the GFDL SPEAR model hindcasts begin in 1991. The ACCESS-S2 model is evaluated from 1991 through 2018, when the hindcasts end (there is a several-year gap before real-time forecasts were operationalized). In the results, the forecast verification focuses on temporal anomaly correlations (AC) between the forecasts and OISSTv2.1 monthly mean data (Huang et al. 2021), but the mean squared error skill score (MSESS) from the NMME is also shown in supplemental Fig. 2.

Finally, through the use of linear regression, teleconnections in 200-hPa geopotential heights are evaluated over 1959–2021 from the ERA5 dataset (Hersbach et al. 2020). Globally, monthly average precipitation anomalies are examined over the ocean and land from the CPC Merged Analysis of Precipitation during 1979–2022 (CMAP; Xie and Arkin 1997). Regionally, station-based gridded monthly average precipitation datasets are also examined during key impact seasons for Australia (June–August) and the United States (January–March) during 1979–2022. The CPC Unified gauge-based analysis is relied upon for calculations focused on the United States (Chen et al. 2008) and the Australian Gridded Climate Data (AGCD) version 2 is used for Australia (Evans et al. 2020). A carbon dioxide (CO_2) index is also examined from the Mauna Loa observatory, which is obtained from NOAA Global Monitoring Laboratory (Keeling et al. 1976).

3. Results

a. *Relative Niño-3.4 index across three observational SST datasets*

For each of the three SST datasets, Fig. 2 displays the Oceanic Niño Index (ONI; top panel), 3-month running average of the tropical mean SST index (middle panel), and Relative Oceanic Niño Index (RONI; bottom panel, defined as the 3-month running average of the relative Niño-3.4 index), each computed with respect to the 1991–2020 climatology for the entire record (note: this figure and all others below are computed with respect to a single climatology). As expected, the datasets are in better agreement in the recent satellite era record (late 1970s onward), with less agreement evident the further back in the historical record that is a result of sparser in situ measurements and therefore greater sensitivity to the chosen SST reconstruction scheme. Over time, there is a positive trend in the ONI index (supplemental Table 1 and supplemental Fig. 3), with more El Niño extremes and fewer La Niña extremes in the recent record. Compared to the ONI, the tropical mean SST index has less variability, but shows a positive trend in all datasets, which more clearly reflects the gradually warming climate. The amplitude of

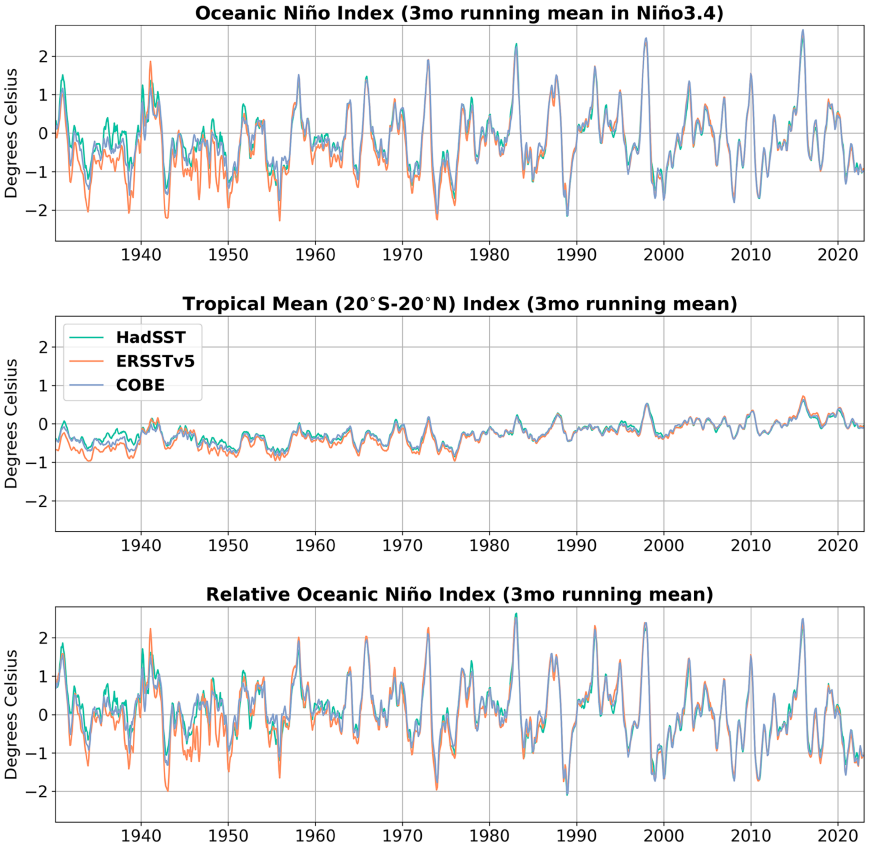

FIG. 2. Values of the (top) Oceanic Niño Index (ONI), (middle) tropical mean SST index, and (bottom) Relative Oceanic Niño Index (RONI) are displayed for three SST datasets (see legend). Data spans 1931–2022 (x axis) and are in units of °C (y axis).

the positive trend in the tropical mean index is larger, and more statistically significant, than the ONI. Therefore, when the two indices are subtracted to form the RONI (Fig. 2), a less discernible, but slightly negative trend emerges. A ~95% confidence interval based on block bootstrapping shows that only the negative trend in HadSST is distinct from zero (supplemental Table 1). Regardless, as in van Oldenborgh et al. (2021), the RONI damps the positive SST trend found in the ONI, making seasonal ENSO variability a more distinctive feature of the time series.

When the tropical mean index is subtracted from the ONI, there is a loss in variance in the resulting time series, which, as discussed in the introduction, is problematic for operational agencies that rely on threshold anomalies to determine the status of ENSO. Therefore, the time series of RONI in Fig. 2 incorporates a scaling factor to match the variance of the RONI to that of the ONI. In forecast and observational data, the scaling method is simpler to use and computationally faster than the regression-based method described in van Oldenborgh et al. (2021). The scaled relative index is defined as

$$\text{Relative ONI} = (\text{ONI} - \text{TropAve}) \times \frac{\sigma_{\text{ONI}}}{\sigma_{(\text{ONI}-\text{TropAve})}},$$

where σ is the standard deviation (1950–2020 in Fig. 2) and the ONI and tropical mean indices are computed relative to a 30-yr climatology (1991–2020 in Fig. 2). The scaling ratio is computed separately for each calendar month/season and is largest in March–May and smallest during July–August (supplemental Fig. 4). The RONI associated with the two inflation methods appear very similar (Fig. 3), but the scaling method results in a RONI variance that more closely matches the original ONI variance, and will be used through the remainder of this study. The scaling ratio is computed by month/season because the variance of the ONI changes substantially by month/season. If used for operational purposes, the scaling ratio should be updated periodically, ideally at the same time the 30-yr climatology is updated, to ensure the relative index has the same variance as the nonrelative index.

One of the advantages of adopting RONI is that the categorization of historical El Niño and La Niña events is less sensitive to the choice of 30-yr climatology. Figure 4 shows heat maps across time (1950–2022) of historical El Niño episodes (in red shading) and La Niña episodes (in blue shading) as defined by NOAA's ±0.5°C threshold and the requirement that ENSO periods last at least five consecutive overlapping seasons. Each column on the x axis represents the use of a different 30-yr climatology period (presented in Fig. 1). The left

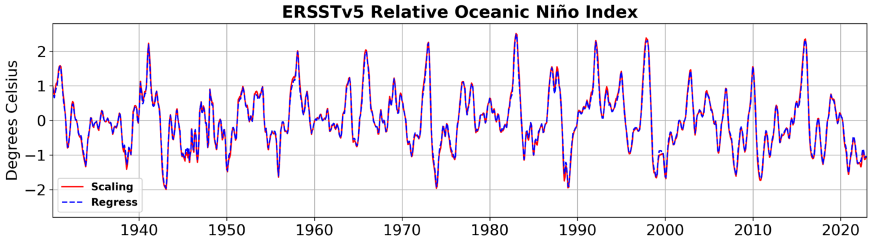

FIG. 3. The Relative Oceanic Niño Index is shown from 1931 through 2022 for the scaling method (red line) and for the van Oldenborgh et al. (2021) regression-based method (dashed blue). Data are from ERSSTv5.

panel shows the historical ENSO classifications based on the ONI (using a single climatology for the entire historical record for each column) and the right panel shows the same for the RONI. For the ONI (left panel), varying the 30-yr climatology has a substantial impact on the classification of past El Niño and La Niña episodes. In particular, using an older climatology (e.g., 1931–60) increases the number of El Niño events and their duration, while reducing the number of La Niña events and their length. Due to the positive trend in the ONI (Fig. 2, top panel), the use of a comparably cooler climatological base period shifts the index toward more positive values. Likewise, using a more recent climatology (e.g., 1991–2020) translates into more frequent and longer-lived La Niña events because of the warmer base period.

In contrast to that for ONI (left panel), the heat map using the RONI (right panel) shows colors that are more horizontally aligned from the first column to the last column, meaning that the historical classification of ENSO episodes is more consistent irrespective of the selected climatology. ERSSTv5 is shown in Fig. 4, and results for the other two SST datasets are found in supplemental Fig. 5. The trends in the other two SST datasets are smaller than that in ERSSTv5 (supplemental Table 1 and supplemental Fig. 3) and as a result show less dependence on climatology than ERSSTv5.

Given the differences among SST datasets, another attractive property of RONI is the modest increase in alignment in the ENSO event classification between ERSSTv5 data and the other two datasets when RONI is used versus the ONI. Figure 5 shows the root-mean-square differences (RMSD) based on the ENSO classification shown in Fig. 4 and supplemental Fig. 5 (with periods of El Niño = +1, neutral = 0, and La Niña = −1). The columns show the RMSD between different SST datasets and the y axis shows the selected 30-yr climatology. The top-left panel is the RMSD for ENSO classifications using the ONI between 1950 and 2022 and the top-right panel shows the same for the RONI. The bottom panel shows the difference between the two top panels. While the reductions are modest, the RMSD between ERSSTv5 and the other two datasets (COBE, HadSST) are mostly either the same (lighter shading) or reduced (blue shading) when the RONI is used. A primary reason for this is the reduction in the trend in ERSSTv5 when RONI is used. Supplemental Fig. 3 and supplemental Table 1 show that ERSSTv5 has a large positive trend in the ONI and, after the tropical mean is subtracted, the resulting RONI has a much smaller trend, which is more comparable to the RONI trends in HadSST and COBE.

b. *Forecast verification with the NMME and ACCESS-S2*

Another important consideration is how skillfully the relative Niño-3.4 index can be predicted. Van Oldenborgh et al. (2021) briefly evaluated two versions of the ECMWF model (S4 and S5) and found that the monthly Niño-3.4 and relative Niño-3.4 indices have similar anomaly correlations for most target months, with the exception of those targeted for boreal spring (March–May), which have slightly lower correlations in the relative index (a difference of 0.3 at most). However, they displayed a single forecast lead time (+2 months) and therefore we extend the evaluation to include all lead times for the six models that comprise the NMME in use at NOAA, and the ACCESS-S2 model in use at BOM. First focusing on the NMME, Fig. 6 shows the anomaly correlation skill score for the monthly Niño-3.4 index (top row), monthly relative Niño-3.4 index (middle row), and the difference (Niño-3.4 AC minus relative Niño-3.4 AC; bottom row). Each panel shows a single NMME model, with target month on the x axis and monthly lead time on the y axis. Two of the models have shorter forecast time horizons (NASA-GEOSS2S and NCEP-CFSv2), and these periods are masked out with gray shading, as are targets and lead times with statistically insignificant skill (5% significance level).

Reflecting the boreal spring predictability barrier, all models show a reduction in correlation for boreal spring start months (initial conditions) that is manifest for target months beginning approximately in May. This lower skill region extends diagonally into the top right corner, illustrating the lower skill found at progressively longer lead times for target months in the last half of the year. The spring predictability barrier is present in both indices, but the bottom panel shows that, for target months in the first third to half of the calendar year, the relative Niño-3.4 index has slightly lower correlations than the Niño-3.4 index (change in correlation coefficient from ~0.1 to 0.3). A sign test (e.g., DelSole and Tippett 2014) applied to the correlations indicates that these differences are statistically significant for only some models and lead times, mostly for March–May targets (at the 5% significance level). For some models (e.g., NCEP-CFSv2, GEM-NEMO5) the period with the largest reduction in skill persists for targets into July, and longer forecast leads generally are associated with a

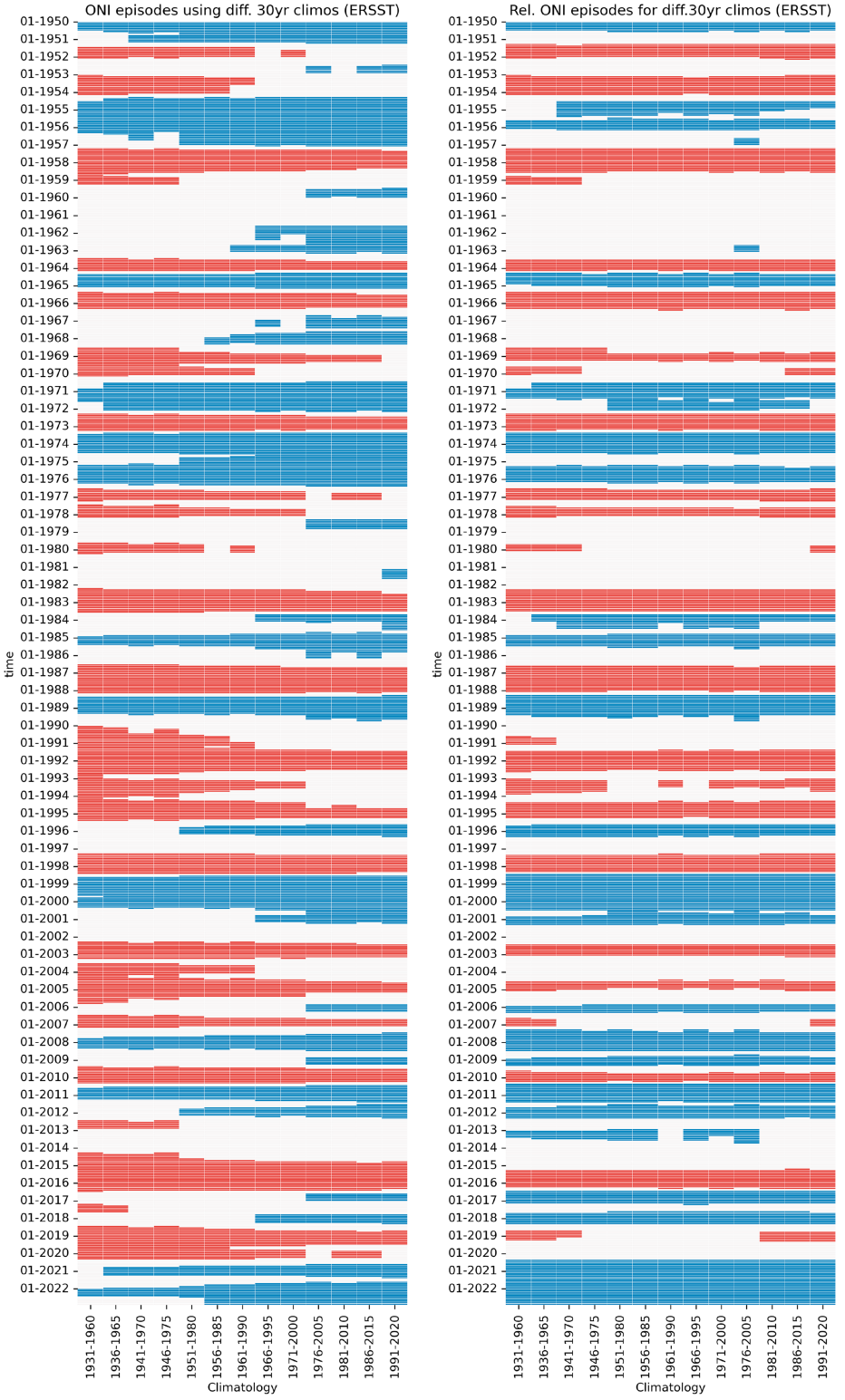

FIG. 4. Heat maps of historical El Niño (red shading) and La Niña (blue shading) episodes as defined by NOAA's ±0.5°C threshold and requirement that ENSO periods last at least five consecutive overlapping seasons. Each column on the *x* axis represents a different 30-yr climatology period. (left) The historical ENSO classifications based on the ONI (using only a single climatology for the entire historical record); (right) as in the left panel, but for the RONI. Data are from ERSSTv5.

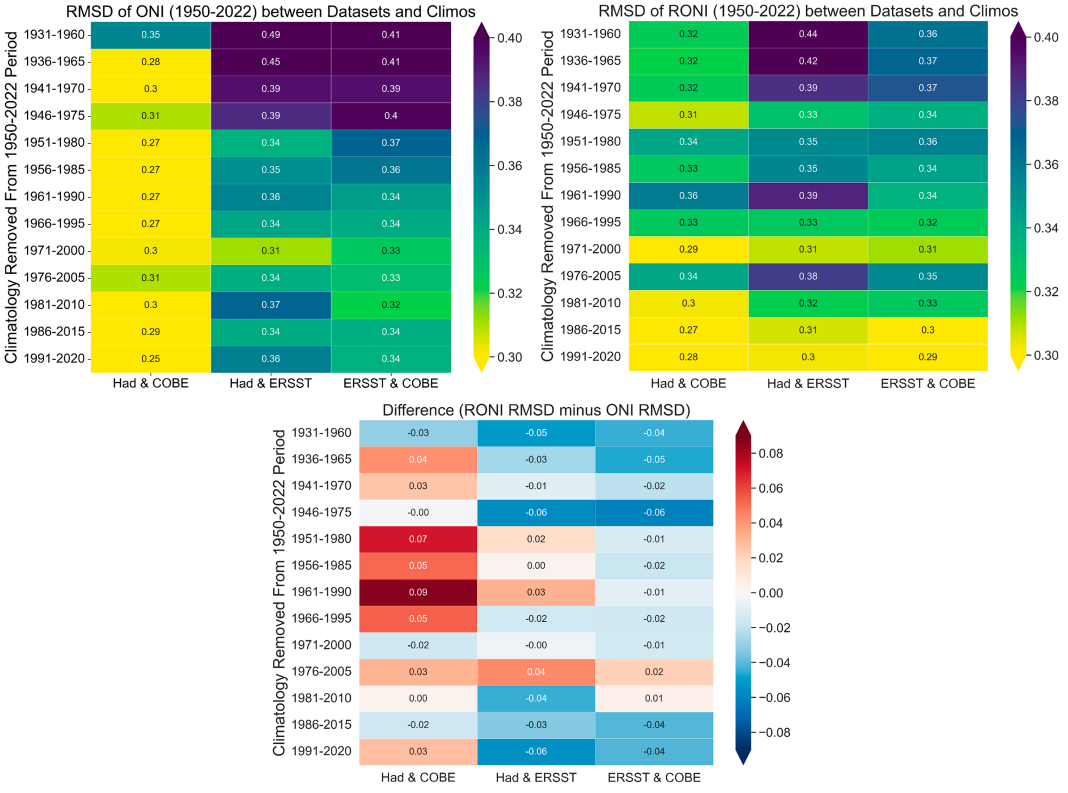

FIG. 5. The root-mean-square differences (RMSD) between each SST dataset (x axis), with the y axis showing overlapping 30-yr climatologies. (top left) The RMSD for the seasonally overlapping ONI values between 1950 and 2022; (top right) as in the top-left panel, but for the RONI. (bottom) The difference between the top two panels.

larger drop in skill, though not exclusively. For instance, NCEP-CFSv2 shows an almost uniform skill reduction at all lead times.

Van Oldenborgh et al. (2021) noted that months with lower skill in the relative Niño-3.4 index tend to be the same months with smaller Niño-3.4 index variance, which can lead to lower skill because trends would play a correspondingly larger role. They argued that the skill of the Niño-3.4 index is therefore slightly inflated due to trends. However, linearly detrending the predicted Niño-3.4 index and then correlating it to the observed Niño-3.4 slightly increases forecast skill (not shown). This implies that the presence of trends, within the Niño-3.4 index itself, does not fully account for a reduction in skill in relative Niño-3.4. Also, for the shorter 1991–2020 model hindcast period, the Niño-3.4 index trend is small and negative. We therefore explore this further in Fig. 7.

In the NMME, Fig. 7 (top row) shows the forecast skill of the tropical mean index, which is subtracted from the Niño-3.4 index to form the relative Niño-3.4 index. The tropical mean index forecast also seems to be influenced by the same boreal springtime barrier that impacts skill in the Niño-3.4 index, which likely stems from the relationship between the tropical mean and Niño-3.4 indices (in models and observations, $r > 0.5$ for January–May). For every model, the highest skill at leads greater than 6 months occurs for target months in the first half of the calendar year, and for spring target months in particular (Fig. 7, top row). To better highlight this seasonal peak in skill in the tropical mean index, the all-months average skill (January–December for each lead time) is subtracted from that of the monthly index, with red (blue) shading indicating where correlations are larger (smaller) in the seasonal cycle relative to other calendar months (Fig. 7, middle panel). For consistency, the same procedure is applied to the difference plot previously shown in the bottom row of Fig. 6 and is now presented in the bottom row of Fig. 7. It is apparent that the seasonality of skill in the tropical mean index (middle row of Fig. 7) largely corresponds with targets/lead times that have higher skill in the Niño-3.4 index compared to the relative Niño-3.4 index. Put another way, the skill reduction that occurs in the relative Niño-3.4 index (vs. Niño-3.4) is at least partially attributable to the fact the tropical mean index is being subtracted, which is removing a component that is both skillful and related to Niño-3.4, particularly during the spring. This component of the Niño-3.4 skill likely reflects, in part, the communication of the tropical Pacific anomalies to remote ocean basins that lags the peak of ENSO (Chiang and Sobel 2002). Conversely, during the last half of the year, when the tropical mean index is comparatively less skillful, subtracting it from the Niño-3.4 index results in a relative Niño-3.4 index that is just as skillful (neutral to slightly blue shaded regions in Fig. 6, bottom row).

Analysis of the ACCESS-S2 model forecasts is largely consistent with the NMME models. Figure 8 displays the equivalent anomaly correlations that were displayed in Fig. 6 (left panel)

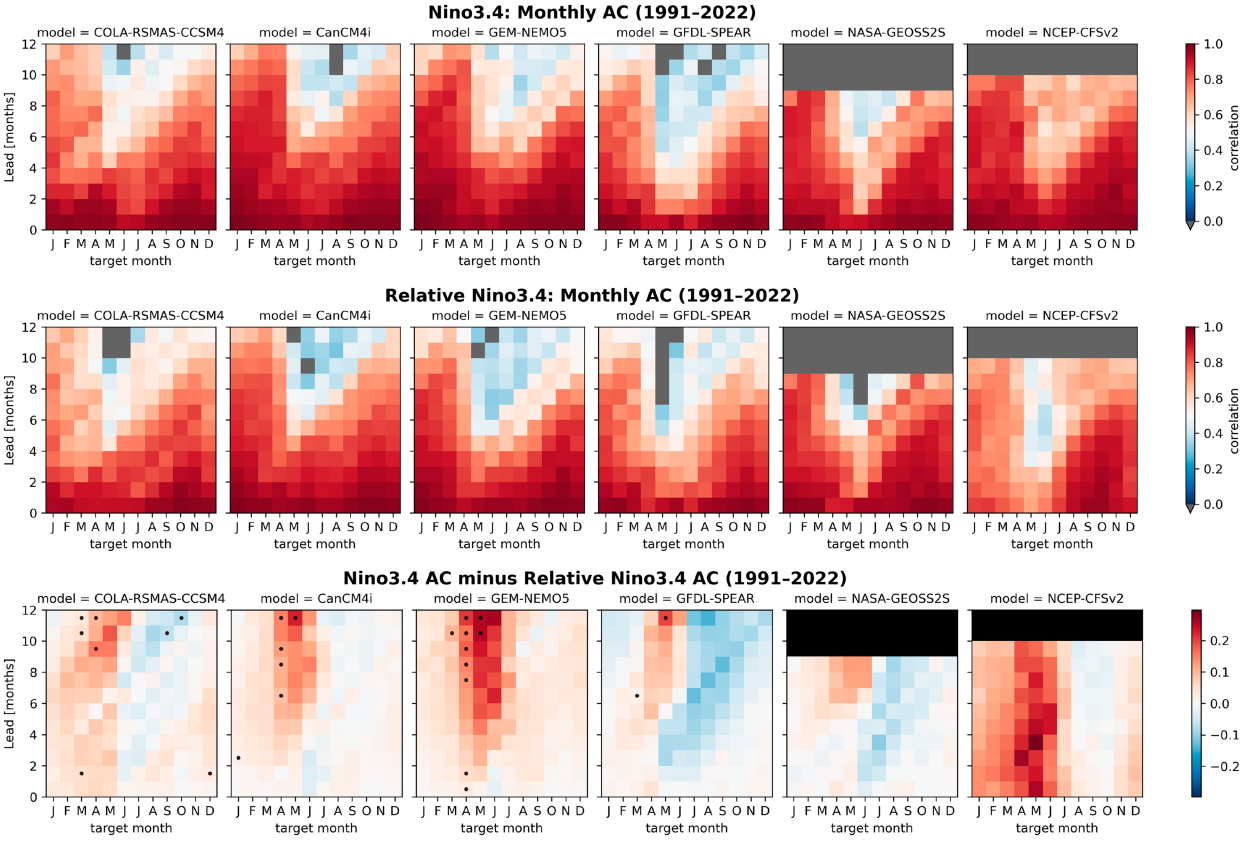

FIG. 6. Anomaly correlation between NMME ensemble-mean forecasts and OISSTv2.1 observations for the (top) monthly Niño-3.4 index and (middle) monthly relative Niño-3.4 index, and (bottom) their difference (Niño-3.4 minus relative Niño-3.4). Each panel shows a single NMME model, with target (validation) month on the x axis and monthly lead time on the y axis. In the top and middle rows, GEOSS2S and NCEP-CFSv2 have shorter forecasts and lead times beyond 9 and 10 months, respectively, are masked out with gray shading, as are targets and lead times with statistically insignificant skill ($p > 0.05$). In the bottom row, dots indicate targets and lead times with statistically significant differences in skill ($p < 0.05$).

and Fig. 7 (right panel). Even though the evaluation periods are not identical (1991–2018 in ACCESS-S2 versus 1991–2022 in NMME), it is clear that ACCESS-S2 shares the same first half-year reduction in skill when a relative Niño-3.4 index is used (Fig. 8, bottom-left panel). The skill of the tropical mean index (Fig. 8, top-right panel) also compares well with the most skillful NMME models (Fig. 7, top row). Subsequently, the reduction in relative Niño-3.4 index skill (Fig. 8, bottom row) clearly coincides with the seasons of higher skill in predicting the tropical mean (Fig. 8, middle-right panel).

c. *Relationships with upper-level circulation anomalies*

Another of the potential advantages of removing the influence of a changing climate in Niño-3.4/ONI is that the new index may better represent the conventional year-to-year ENSO signal in the global circulation. A typical measure of global climate change is the tropospheric concentration of carbon dioxide as indicated by the CO_2 index (Fig. 9), which has a very steady increasing trend. However, regional climate change is often not expressed as a change related linearly to increasing carbon dioxide. Indeed, the relative Niño-3.4/ONI is uncorrelated with the CO_2 index, whereas the CO_2 index and tropical mean SST index have a similar increasing trend ($r = 0.7$; Fig. 9). This is explained by the fact that the tropically averaged surface conditions set the temperature of the free troposphere. Thus, subtracting out the tropical mean SST index from Niño-3.4/ONI, to better isolate regions of local instability, also helps to reduce the influence of regional climate change on the Niño-3.4/ONI. Van Oldenborgh et al. (2021) thus argue that the relative ONI isolates a purer ENSO signal, unencumbered by the low-frequency influence of climate change.

In part because the tropical mean SST index incorporates the influence of CO_2 and its radiative effects, it is a key predictor of the tropical circulation and anomalous geopotential heights. Figure 10 shows overlapping seasonal 200-hPa geopotential height (GPH) anomalies regressed onto the ONI (top panel), the relative ONI (middle panel), and the difference between the top and middle panels (bottom panel). Both ONI and relative ONI patterns exhibit the classic ENSO teleconnection stemming from the tropical Pacific and influencing the middle-to-high latitudes (Horel and Wallace 1981). However, the ONI pattern is

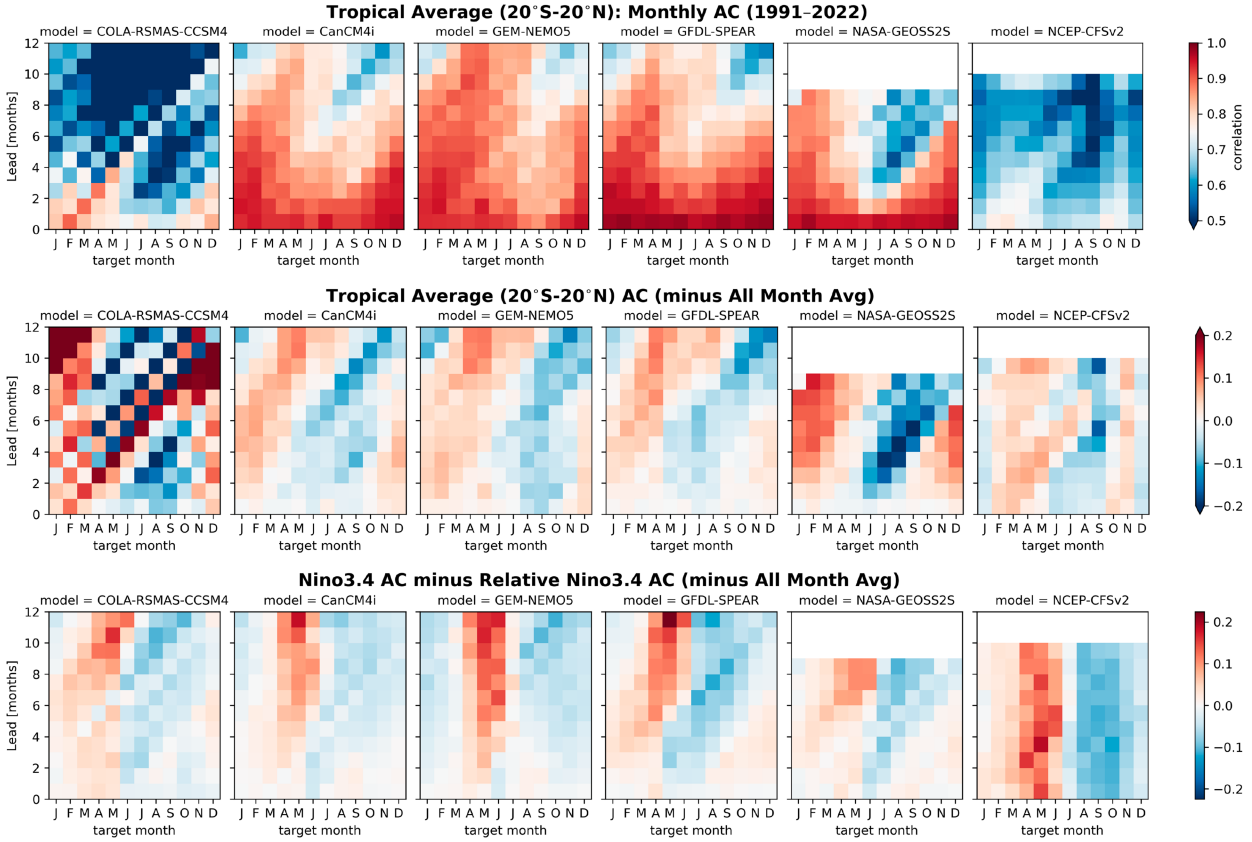

FIG. 7. (top) Anomaly correlation between NMME ensemble-mean forecasts and OISSTv2.1 observations for the monthly tropical mean (20°S–20°N) index. (middle) The skill with the all-month average subtracted from the tropical mean index, highlighting the seasonality of skill. Red (blue) shading indicates where correlations are largest (smallest) in the seasonal cycle relative to other calendar months. (bottom) As in the bottom row in Fig. 6, except with the all-month average subtracted out.

characterized by widespread, positive GPH anomalies over the globe, with the exception of the high latitudes of the Southern Hemisphere. The relative ONI pattern is associated with a reduction of positive height anomalies compared to the ONI, especially in the tropical latitudes, which reflects the consequence of subtracting out the tropical average SST. Additionally, in the relative ONI plot, the area covered by the positive height anomalies appears to be more equally balanced with regions of negative height anomalies, hinting that conventional ENSO variability is being isolated.

To better understand the contributions to the difference map between the ONI and RONI (Fig. 10 bottom panel), we employ a three-predictor linear regression equation (Fig. 11). Because CO_2 is a key contributor to climate change, we select this index as a predictor. We also include the components of RONI: tropical mean SST index and the ONI, as the second and third predictors. For the seasonal averages used here, a smoothed global mean temperature index can be substituted for the CO_2 index, with indistinguishable results.

As might be expected, the CO_2 and the tropical mean SST indices are associated with widespread, positive geopotential height anomalies (top two panels of Fig. 11). However, because CO_2 and the tropical mean are correlated (Fig. 9), the two maps exhibit a high degree of collinearity and are split with positive height anomalies dominating different regions. In fact, the tropical mean index is equally driven by ENSO (as measured by ONI) and CO_2. While not shown, the time series of the tropical mean is nearly reproduced ($r = 0.9$) by linearly combining the time series of the ONI and CO_2. Thus, the tropical mean index isolates the regional expression of climate change (CO_2) plus ENSO variability, and is critical to explaining the global 200-hPa height anomalies. If only CO_2 is used in combination with the ONI (a two-predictor regression), CO_2 is insufficient to explain the positive height differences in Fig. 10 (bottom panel), especially over the tropics. Consequently, in order to sufficiently explain the positive height differences in Fig. 10 (bottom panel), both CO_2 and the tropical mean indices must be included as predictors. Supplemental Fig. 6 (bottom panels) confirms the summation of these regression maps (CO_2 + tropical mean) closely matches the bottom panel of Fig. 10.

While CO_2 and tropical mean index collectively explain the radiatively forced climate change signal in the global height anomalies, the final predictor, targeting ENSO variability, strongly resembles the height anomalies described by relative ONI (cf. Fig. 10, middle panel with Fig. 11, bottom). This indicates the

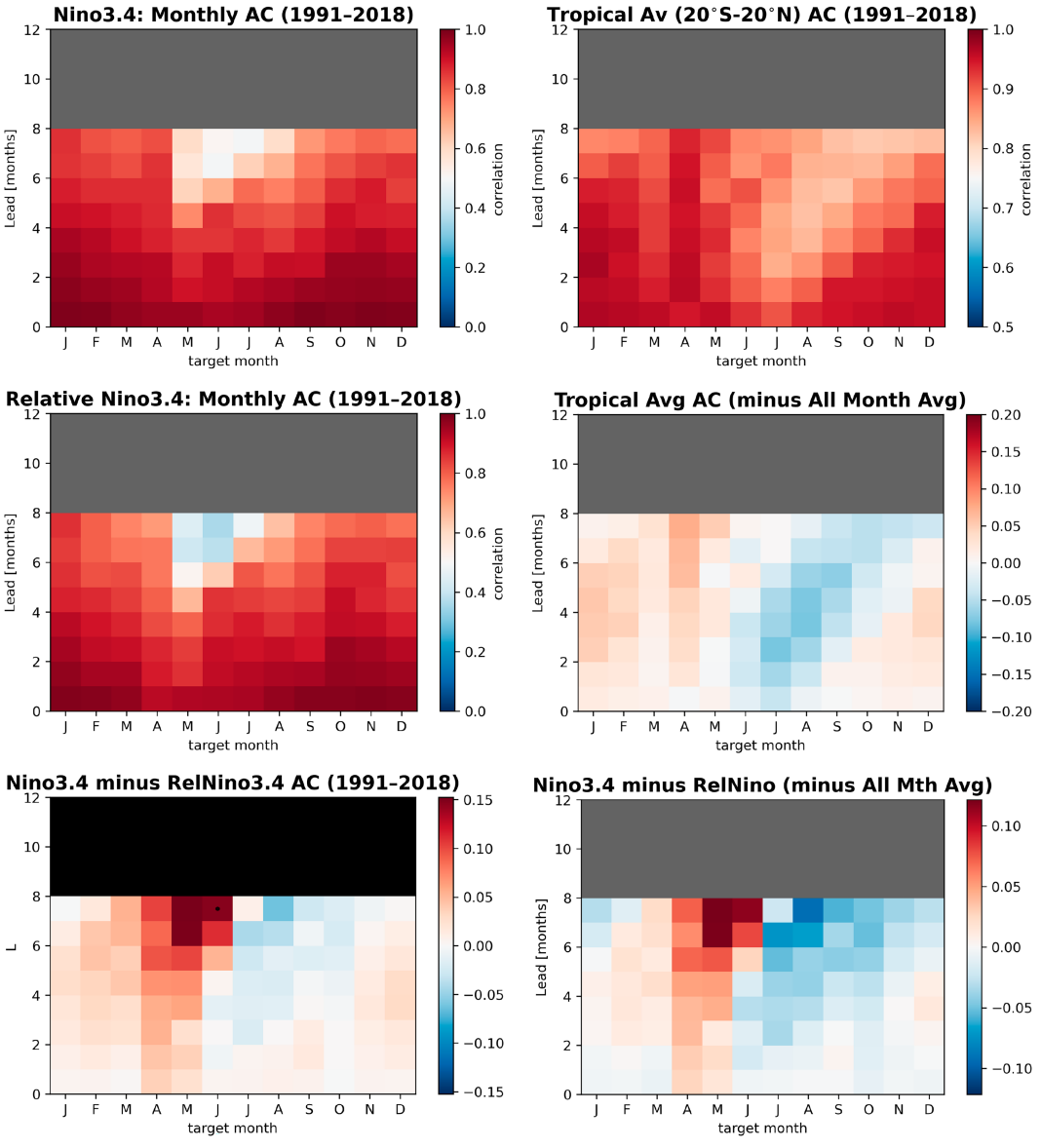

FIG. 8. As in (left) Fig. 6 and (right) Fig. 7, except showing the anomaly correlations from the BOM ACCESS-S2 model.

process of subtracting out the tropical mean SST from the ONI reduces the radiatively forced climate change component that is intrinsic to the ONI. The smaller positive height anomalies indicate that the relative ONI better reflects ENSO only impacts.

d. Relationships with precipitation anomalies

The relative ONI index also sharpens the tropical Pacific precipitation anomaly dipole that is a signature of ENSO-related changes in the equatorial overturning circulation (e.g., Ádames and Wallace 2017). Figure 12 shows the January–March (left panel) and June–August (right panel) global CMAP precipitation anomalies regressed onto the ONI (top panel) and the relative ONI (middle panel), and the difference between the two (RONI minus ONI; bottom panel). Compared to the ONI, the relative ONI regression maps (middle panel) are associated with more amplified precipitation anomalies over the Maritime Continent region and central/western Pacific Ocean. The difference maps reveal the stronger anomalies of the RONI overlaid with the typical anomalous tropical dipole (shown with contours). In the boreal winter months, the pattern is more zonally oriented, whereas in the boreal summer months the anomalous dipole shifts northwestward due to increased solar heating over the Northern Hemisphere. Despite the shifts in the seasonality of the tropical dipole, the relative ONI makes both the positive anomalies wetter and the negative anomalies drier. Therefore, the relative index more strongly identifies the zonal asymmetries in the tropical precipitation anomalies, tied to the coupled feedbacks of the ENSO cycle.

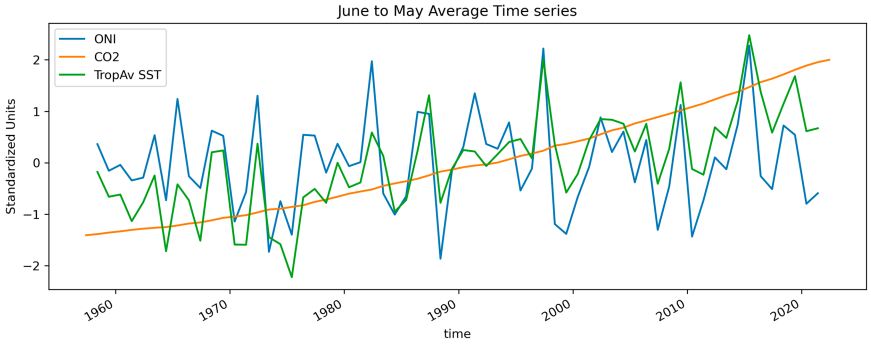

FIG. 9. Standardized June–May (annual) averaged index values of the nonrelative Oceanic Niño Index (ONI; blue line), CO_2 index (orange line), and tropical mean SST index (green line). The June–May average is based on Tippett and L'Heureux (2020). Data are shown from 1959 to 2021. SST indices are based on HadSST.

The relative ONI does not explain more variance in precipitation anomalies everywhere across all seasons, but it does add some modest explanatory power in some key ENSO regions during seasons of peak impact. Focusing on Australia (June–August) and the contiguous United States (January–March), Fig. 13 displays the correlation of precipitation anomalies with the ONI (top panel), the relative ONI (middle panel), and the percent variability explained (correlation coefficient squared, ×100) difference between the relative and nonrelative indices. During their respective winter seasons,

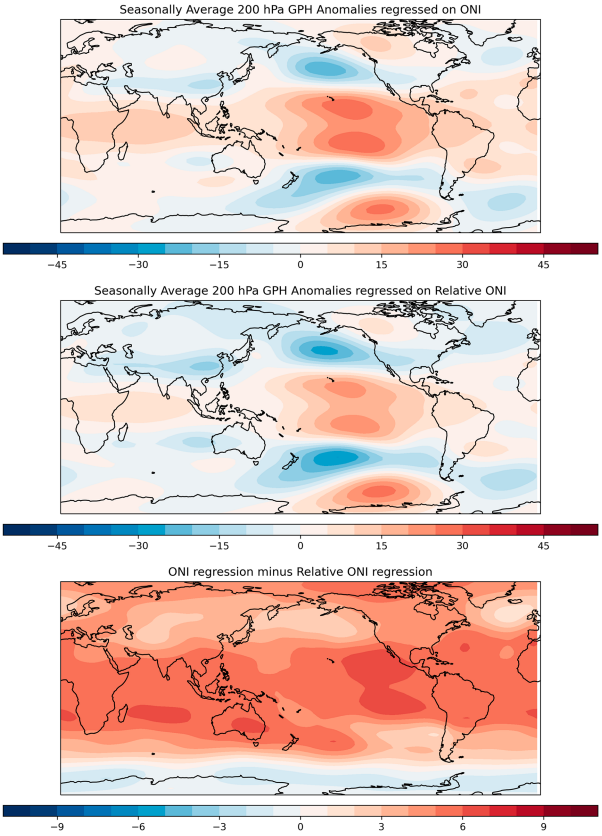

FIG. 10. Overlapping seasonal average 200-hPa geopotential height (GPH) anomalies (m) regressed onto (top) the ONI and (middle) the relative ONI, and (bottom) the difference between the top and middle panels. GPH data are based on ERA5 and SST data are based on HadSST from 1959 to 2021.

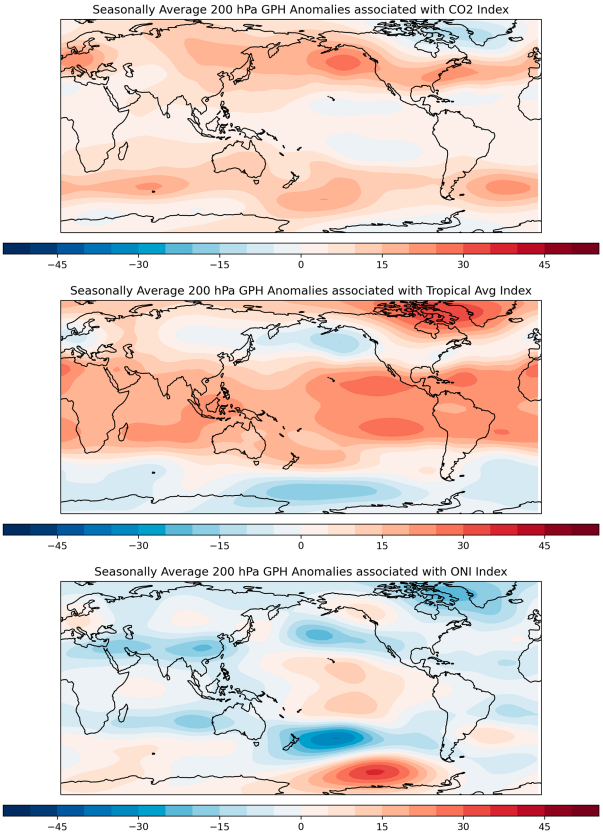

FIG. 11. Three-predictor multiple linear regression patterns to predict overlapping seasonal average 200-hPa geopotential height anomalies (m) using a (top) CO_2 index, (middle) tropical mean SST index, and (bottom) nonrelative ONI. GPH data are based on ERA5, and SST data are based on HadSST from 1959 to 2021.

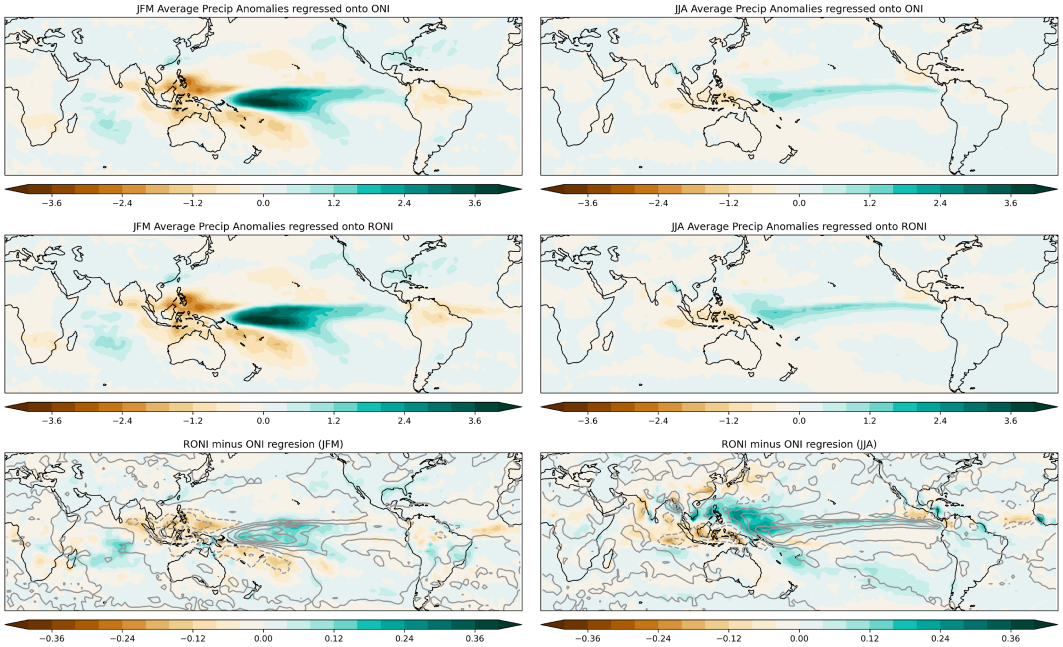

FIG. 12. (left) January–March average precipitation anomalies (mm day^{-1}) regressed onto the (top) ONI and (middle) RONI, and (bottom) their difference. (right) As in the left column, but for June–August. The contours in the bottom panels are duplicated from the top panels. Precipitation anomalies from CPC Merged Analysis of Precipitation over 1979–2022.

the relative ONI appears to add ~5%–10% more explained variability over the positively correlated southern regions of the United States and over Queensland and New South Wales in eastern Australia. In the United States the seasonal precipitation of the southwestern states is especially well captured by the relative index, and the intensity of this signal persists through the February–April and March–May seasons as well (not shown). For Australia the enhanced variance explained continues during July–September and August–October (not shown), which is consistent with the ENSO influence shown in Risbey et al. (2009).

4. Conclusions and discussion

Because classifying El Niño and La Niña events in the historical record requires a climatology, it has become increasingly imperative to reckon with climate change in ENSO monitoring and forecasting tools. SSTs across the tropical Pacific are undoubtedly influenced by past climate change, and, even if it is not fully understood how exactly SSTs will change in the future, lower-frequency variability in SSTs must be recognized and addressed (Lee et al. 2022; Maher et al. 2023). Relative SST provides a useful paradigm for the monitoring and prediction of the oceanic component of ENSO, mainly because it does not strongly depend on the choice of a climatology. Across multiple SST datasets, and different 30-yr climatologies, the historical classification of ENSO events is more robust when a relative Niño-3.4 index/ONI is used.

Further, we have shown that predictions of relative Niño-3.4/ONI remain skillful across several state-of-the-art climate models from the North American Multimodel Ensemble (NMME) and ACCESS-S2. While there is a slight reduction in skill (correlations are ~0.1–0.3 lower) in the relative index, especially for verification times in the early half of the year, it is likely that the classic Niño-3.4 index is deriving some skill from lower-frequency changes versus seasonal-to-interannual ENSO dynamics. As evidence, the tropical mean index, which is subtracted from Niño-3.4/ONI to form the relative index, has higher skill during the first half of the year as well. Because the tropical mean index is correlated to Niño-3.4 ($r > 0.5$), the subtraction results in some removal of prediction skill during the first half of the calendar year. In contrast, in the last half of the year, the relative Niño-3.4 index is just as skillful as the nonrelative index. Ultimately, removing the lower-frequency component of the Niño-3.4 index is beneficial to certain users because this part does not impact the global climate in the same way as the seasonal-to-interannual component.

To establish that the relative Niño-3.4 index captures variability more strongly associated with seasonal ENSO teleconnections, we evaluated relationships with the global mean circulation and precipitation anomalies. ONI relationships with 200-hPa geopotential height are characterized by higher heights across most of the globe compared to the relative index. Also, a three-predictor regression with CO_2, tropical mean SST, and the ONI as predictors reveals that the height pattern associated with the ONI, independent of the other two predictors, strongly resembles that of the relative ONI. This finding suggests that radiative effects, embedded within the CO_2 and tropical mean SST influences, are leaking into

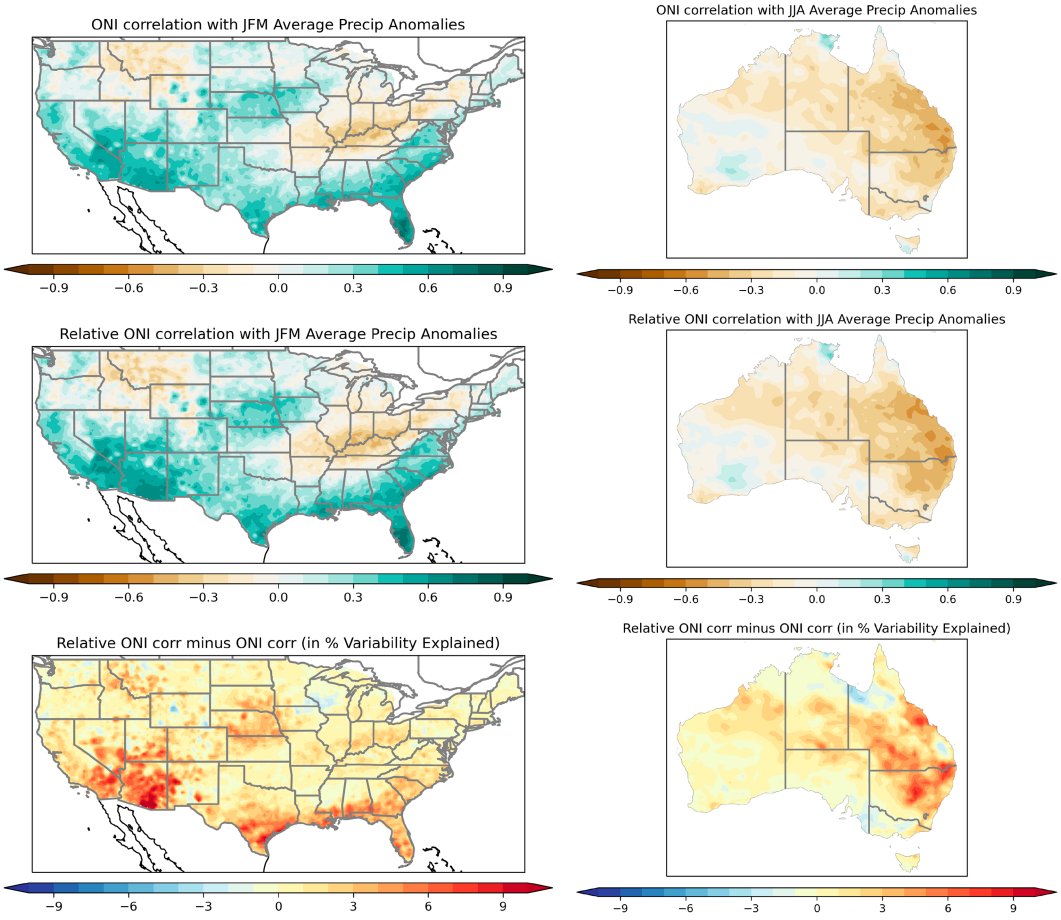

FIG. 13. (left) Over the contiguous United States, correlation of January–March average precipitation with (top) ONI and (middle) RONI; (bottom) the percent variance explained by RONI minus the percent variance explained by ONI. (right) As in the left column, but for Australia during June–August. Precipitation anomalies from CPC Unified gauge-based analysis (for the United States) and Australian Gridded Climate data version 2 over 1979–2022.

the nonrelative index. Additionally, the pattern of tropical Pacific precipitation anomalies becomes sharper when a relative index is used. During their respective winter/spring seasons, the relative index describes about ~5%–10% more precipitation variability over portions of the southern United States and eastern Australia. All considered, a relative SST index appears to better isolate the expected ENSO teleconnections, without mixing in signals from background climate change or low-frequency variability.

For some purposes, such as the prediction of seasonal temperature and precipitation, it is fundamental to consider lower-frequency climate changes and ENSO collectively. But for attribution and for monitoring of the ENSO phenomenon itself, it is problematic to have climate change incorporated within the Niño-3.4 index/ONI. Without an adjustment made to the traditional ENSO index, a periodic reshuffling of historically classified El Niño and La Niña events is likely to occur, which may not reflect baseline conditions experienced at the time of the event. This paper expands upon the initial work of van Oldenborgh et al. (2021) and further justifies the use and adoption of a relative SST index for monitoring and prediction. As they previously cautioned, in the future, if there are significant divergences between the tropical mean state and trends in the Niño indices, then this index will need to be re-evaluated. We hope this work motivates additional studies and simulations of these indices in a changing climate.

Acknowledgments. We thank Dan Harnos (NOAA CPC), Eun-Pa Lim (BOM), Zhi-Weng Chua (BOM), and three anonymous reviewers for their comments, which helped to improve the manuscript.

Data availability statement. The NMME model data analyzed for this study can be found in the International Research Institute for Climate and Society data library https://iridl.ldeo.columbia.edu/SOURCES/.Models/.NMME/ and precipitation data were provided by the NOAA Physical Sciences Laboratory, Boulder, Colorado, USA, from their website at https://psl.noaa.gov. The CO_2 data came from the NOAA Global Monitoring Laboratory, from their website at https://gml.noaa.gov/.

ERA5 data were retrieved from the Copernicus Climate Data Store, from their website at https://cds.climate.copernicus.eu/cdsapp. Australian Gridded Climate data were obtained from the Australian government, at their website https://portal.ga.gov.au/. ACCESS-S2 data are published on the National Computational Infrastructure (NCI) and are available for research purposes from https://geonetwork.nci.org.au/geonetwork/srv/eng/catalog.search#/metadata/f3311_4920_0252_8073. Python code to calculate the relative ONI index from ERSSTv5 is available at https://github.com/michellelheureux/Relative-SST/ and from the NMME predictions at https://github.com/mktippett/NMME/.

REFERENCES

Ádames, A. F., and J. M. Wallace, 2017: On the tropical atmospheric signature of El Niño. *J. Atmos. Sci.*, **74**, 1923–1939, https://doi.org/10.1175/JAS-D-16-0309.1.

Back, L. E., and C. S. Bretherton, 2009: On the relationship between SST gradients, boundary layer winds, and convergence over the tropical oceans. *J. Climate*, **22**, 4182–4196, https://doi.org/10.1175/2009JCLI2392.1.

Barnston, A. G., M. Chelliah, and S. B. Goldenberg, 1997: Documentation of a highly ENSO-related SST region in the equatorial Pacific: Research note. *Atmos.–Ocean*, **35**, 367–383, https://doi.org/10.1080/07055900.1997.9649597.

Becker, E. J., B. P. Kirtman, M. L'Heureux, Á. G. Muñoz, and K. Pegion, 2022: A decade of the North American Multimodel Ensemble (NMME): Research, application, and future directions. *Bull. Amer. Meteor. Soc.*, **103**, E973–E995, https://doi.org/10.1175/BAMS-D-20-0327.1.

Bjerknes, J., 1969: Atmospheric teleconnections from the equatorial Pacific. *Mon. Wea. Rev.*, **97**, 163–172, https://doi.org/10.1175/1520-0493(1969)097<0163:ATFTEP>2.3.CO;2.

Chen, M., W. Shi, P. Xie, V. B. S. Silva, V. E. Kousky, R. W. Higgins, and J. E. Janowiak, 2008: Assessing objective techniques for gauge-based analyses of global daily precipitation. *J. Geophys. Res.*, **113**, D04110, https://doi.org/10.1029/2007JD009132.

Chiang, J. C. H., and A. H. Sobel, 2002: Tropical tropospheric temperature variations caused by ENSO and their influence on the remote tropical climate. *J. Climate*, **15**, 2616–2631, https://doi.org/10.1175/1520-0442(2002)015<2616:TTTVCB>2.0.CO;2.

DelSole, T., and M. K. Tippett, 2014: Comparing forecast skill. *Mon. Wea. Rev.*, **142**, 4658–4678, https://doi.org/10.1175/MWR-D-14-00045.1.

Evans, A., D. Jones, R. Smalley, and S. Lellyett, 2020: An enhanced gridded rainfall analysis scheme for Australia. Bureau Research Rep. 041, 35 pp., http://nla.gov.au/nla.obj-2786078795.

Gamble, F., G. Beard, A. Watkins, D. Jones, C. Ganter, V. Webb, and A. Evans, 2017: Tracking the El Niño-Southern Oscillation in real-time: A staged communication approach to event onset. *J. South. Hemisphere Earth Syst. Sci.*, **67**, 64–78, https://doi.org/10.22499/3.6702.001.

Hersbach, H., and Coauthors, 2020: The ERA5 global reanalysis. *Quart. J. Roy. Meteor. Soc.*, **146**, 1999–2049, https://doi.org/10.1002/qj.3803.

Horel, J. D., and J. M. Wallace, 1981: Planetary-scale atmospheric phenomena associated with the southern oscillation. *Mon. Wea. Rev.*, **109**, 813–829, https://doi.org/10.1175/1520-0493(1981)109<0813:PSAPAW>2.0.CO;2.

Huang, B., and Coauthors, 2017: Extended Reconstructed Sea Surface Temperature, version 5 (ERSSTv5): Upgrades, validations, and intercomparisons. *J. Climate*, **30**, 8179–8205, https://doi.org/10.1175/JCLI-D-16-0836.1.

——, C. Liu, V. Banzon, E. Freeman, G. Graham, B. Hankins, T. Smith, and H.-M. Zhang, 2021: Improvements of the Daily Optimum Interpolation Sea Surface Temperature (DOISST) version 2.1. *J. Climate*, **34**, 2923–2939, https://doi.org/10.1175/JCLI-D-20-0166.1.

Ishii, M., A. Shouji, S. Sugimoto, and T. Matsumoto, 2005: Objective analyses of sea-surface temperature and marine meteorological variables for the 20th century using ICOADS and the Kobe Collection. *Int. J. Climatol.*, **25**, 865–879, https://doi.org/10.1002/joc.1169.

Izumo, T., J. Vialard, M. Lengaigne, and I. Suresh, 2020: Relevance of relative sea surface temperature for tropical rainfall interannual variability. *Geophys. Res. Lett.*, **47**, e2019GL086182, https://doi.org/10.1029/2019GL086182.

Johnson, N. C., and S.-P. Xie, 2010: Changes in the sea surface temperature threshold for tropical convection. *Nat. Geosci.*, **3**, 842–845, https://doi.org/10.1038/ngeo1008.

——, and Y. Kosaka, 2016: The impact of eastern equatorial Pacific convection on the diversity of boreal winter El Niño teleconnection patterns. *Climate Dyn.*, **47**, 3737–3765, https://doi.org/10.1007/s00382-016-3039-1.

Keeling, C. D., R. B. Bacastow, A. E. Bainbridge, C. A. Ekdahl Jr., P. R. Guenther, L. S. Waterman, and J. F. S. Chin, 1976: Atmospheric carbon dioxide variations at Mauna Loa Observatory, Hawaii. *Tellus*, **28**, 538–551, https://doi.org/10.1111/j.2153-3490.1976.tb00701.x.

Kirtman, B. P., and Coauthors, 2014: The North American Multimodel Ensemble: Phase-1 seasonal-to-interannual prediction; phase-2 toward developing intraseasonal prediction. *Bull. Amer. Meteor. Soc.*, **95**, 585–601, https://doi.org/10.1175/BAMS-D-12-00050.1.

Lee, S., M. L'Heureux, A. T. Wittenberg, R. Seager, P. A. O'Gorman, and N. C. Johnson, 2022: On the future zonal contrasts of equatorial Pacific climate: Perspectives from observations, simulations, and theories. *npj Climate Atmos. Sci.*, **5**, 82, https://doi.org/10.1038/s41612-022-00301-2.

L'Heureux, M. L., and Coauthors, 2017: Observing and predicting the 2015/16 El Niño. *Bull. Amer. Meteor. Soc.*, **98**, 1363–1382, https://doi.org/10.1175/BAMS-D-16-0009.1.

Li, X., Z.-Z. Hu, R. Ding, and Y. Liu, 2023: Which ENSO index best represents its global influences? *Climate Dyn.*, **61**, 4899–4913, https://doi.org/10.1007/s00382-023-06804-9.

Maher, N., and Coauthors, 2023: The future of the El Niño–Southern Oscillation: Using large ensembles to illuminate time-varying responses and inter-model differences. *Earth Syst. Dyn.*, **14**, 413–431, https://doi.org/10.5194/esd-14-413-2023.

Nguyen, H., C. Lucas, M. Wheeler, and A. Watkins, 2022: Summary of a workshop on ENSO/IOD alert systems for a warming world held 16–17 August 2022. Bureau Research Rep. 072, 12 pp., http://nla.gov.au/nla.obj-3136569121.

NOAA CPC, 2023: Cold and warm ENSO episodes by season. NOAA, accessed 30 June 2023, https://www.cpc.ncep.noaa.gov/products/analysis_monitoring/ensostuff/ONI_v5.php.

Ramsay, H. A., and A. H. Sobel, 2011: Effects of relative and absolute sea surface temperature on tropical cyclone potential intensity using a single-column model. *J. Climate*, **24**, 183–193, https://doi.org/10.1175/2010JCLI3690.1.

Rayner, N. A., D. E. Parker, E. B. Horton, C. K. Folland, L. V. Alexander, D. P. Rowell, E. C. Kent, and A. Kaplan, 2003:

Global analyses of sea surface temperature, sea ice, and night marine air temperature since the late nineteenth century. *J. Geophys. Res.*, **108**, 4407, https://doi.org/10.1029/2002JD002670.

Risbey, J. S., M. J. Pook, P. C. McIntosh, M. C. Wheeler, and H. H. Hendon, 2009: On the remote drivers of rainfall variability in Australia. *Mon. Wea. Rev.*, **137**, 3233–3253, https://doi.org/10.1175/2009MWR2861.1.

Sobel, A. H., I. M. Held, and C. S. Bretherton, 2002: The ENSO signal in tropical tropospheric temperature. *J. Climate*, **15**, 2702–2706, https://doi.org/10.1175/1520-0442(2002)015<2702:TESITT>2.0.CO;2.

Tippett, M. K., and M. L. L'Heureux, 2020: Low-dimensional representations of Niño 3.4 evolution and the spring persistence barrier. *npj Climate Atmos. Sci.*, **3**, 24, https://doi.org/10.1038/s41612-020-0128-y.

Turkington, T., B. Timbal, and R. Rahmat, 2019: The impact of global warming on sea surface temperature based El Niño-Southern Oscillation monitoring indices. *Int. J. Climatol.*, **39**, 1092–1103, https://doi.org/10.1002/joc.5864.

van Oldenborgh, G. J., H. Hendon, T. Stockdale, M. L'Heureux, E. C. de Perez, R. Singh, and M. van Aalst, 2021: Defining El Niño indices in a warming climate. *Environ. Res. Lett.*, **16**, 044003, https://doi.org/10.1088/1748-9326/abe9ed.

Vecchi, G. A., and B. J. Soden, 2007: Global warming and the weakening of the tropical circulation. *J. Climate*, **20**, 4316–4340, https://doi.org/10.1175/JCLI4258.1.

Wedd, R., and Coauthors, 2022: ACCESS-S2: The upgraded Bureau of Meteorology multi-week to seasonal prediction system. *J. South. Hemisphere Earth Syst. Sci.*, **72**, 218–242, https://doi.org/10.1071/ES22026.

WMO, 2017: World Meteorological Organization guidelines on the calculation of climate normals. WMO-1203, 18 pp., https://library.wmo.int/doc_num.php?explnum_id=4166.

Xie, P., and P. A. Arkin, 1997: Global precipitation: A 17-year monthly analysis based on gauge observations, satellite estimates, and numerical model outputs. *Bull. Amer. Meteor. Soc.*, **78**, 2539–2558, https://doi.org/10.1175/1520-0477(1997)078<2539:GPAYMA>2.0.CO;2.